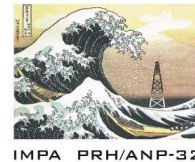


Masters dissertation

Asymptotic Blowup Solutions in MHD Shell Model of Turbulence

Guilherme Tegoni Goedert



Advisor: Alexei Mailybaev, IMPA

July 26, 2016

Dissertação preparada no Instituto Nacional de Matemática Pura e Aplicada como requisito parcial para a obtenção do título de Mestre em Matemática: Opção Matemática Computacional e Modelagem.

Banca examinadora:

Prof. Alexei A. Mailybaev
Orientador
IMPA

Prof. Dan Marchesin
IMPA

Prof. Enrique Ramiro Pujals
IMPA

Prof. Fábio Antonio Tavares Ramos
UFRJ

Data da defesa, 28 de junho de 2016.
Rio de Janeiro, RJ, Brasil.

Dedicatória

À minha família, Moacira, Elsion, Letícia, Beethoven e Mel, além de todos sem os quais este trabalho não seria concluído.

Resumo

Este trabalho considera o problema de formação de singularidades em tempo finito (blowup) em um modelo shell de turbulência magnetohidrodinâmica sob a perspectiva de sistemas dinâmicos. Começamos ao provar um critério de blowup similar ao teorema de Beale-Kato-Majda. O restante de nossa análise é baseada em um esquema de renormalização que leva o tempo de blowup para infinito. Esta transformação associa o blowup a um atrator do sistema renormalizado, construído a partir de seu mapa de Poincaré. Desta forma, nós não apenas descrevemos a estrutura do blowup, como também explicamos sua universalidade. Seguindo este método, mostramos que o blowup possui estrutura caótica para alguns parâmetros. Além disso, nós observamos, para um modelo específico, o interessante efeito de coexistência entre diferentes cenários de blowup, os quais são então selecionados com base nas condições iniciais.

Abstract

This work considers the problem of finite time singularities (blowup) in a shell model of magnetohydrodynamic (MHD) turbulence from a dynamical system standpoint. First, we prove a blowup criterion similar to the Beale-Kato-Majda theorem. Further analysis is based on a renormalization scheme which takes blowup time to infinity. This transformation associates the blowup to an attractor of the renormalized system, found from its Poincaré map. This way, we not only describe the blowup structure but also explain its universality. Following this approach, we show that, for some parameter values, the blowup has a chaotic structure. Moreover, we observe an interesting effect of coexisting blowup scenarios in a specific model, which are selected based on initial conditions.

Contents

1	Introduction	1
1.1	Thesis overview	1
1.2	Motivation and Underlying Ideas	2
1.3	Modelling	3
1.3.1	Hydrodynamic Incompressible Flow	3
1.3.2	Magnetohydrodynamic Flow	4
1.3.3	Shell Models	5
1.4	Blowup	6
2	MHD Turbulence Shell Models and Blowup	10
2.1	Model	10
2.2	Local existence of solutions and blowup	11
3	Renormalization and Symmetry	14
3.1	Renormalization Scheme	14
3.2	Symmetry	16
4	Asymptotic Blowup Solution of a Hydrodynamic Model	18
4.1	Numerical simulation	18
4.2	Asymptotic Blowup Solution	20
5	Attractors	23
5.1	Poincaré Maps	23
5.2	Attractors	26
5.3	Bifurcation Diagrams	31
6	Asymptotic Blowup Solution of an MHD Shell Model	35
6.1	Self-similar Blowup Solutions	35

6.2	Periodic Blowup Solutions	38
6.3	Chaotic Blowup Solutions	41
7	Conclusion	45

Chapter 1

Introduction

1.1 Thesis overview

This thesis is organized in five main chapters, aside from the Introduction and Conclusion.

In the Introduction, Chapter 1, we give a brief description of important problems in fluid dynamics theory that motivate this work. Then we describe the models involved and present the blowup phenomenon through some classical examples.

Chapter 2 is focused on the magnetohydrodynamic shell model over which this thesis was developed. We properly define blowup in this model and prove a criterion for its occurrence, similar to the Beale-Kato-Majda theorem. In Chapter 3 we define a renormalization scheme, which takes blowup time to infinity in the renormalized counterpart of the model studied.

In Chapter 4, we pay attention to a pure hydrodynamic shell model, obtained from identically null initial condition for the magnetic shell variables. We study how some previous works built asymptotic solutions of this model near blowup from travelling wave limiting solutions of its associated renormalized model. In Chapter 5, we return to a detailed study of the limiting solutions of our renormalized MHD model in terms of the attractors of its Poincaré map. These results are then used in Chapter 6 to generalize the results of Chapter 4 to the blowup description for the original MHD shell model.

At the end, we provide a list of publications and conference presentations on the topic of this dissertation.

1.2 Motivation and Underlying Ideas

Turbulence has always been amongst the most intimidating and captivating phenomena in nature. While its ubiquitous character makes a complete theory of turbulent flow an intellectual treasure trove for mathematicians, physicists and engineers, its mercurial behaviour has thwarted any such endeavour.

Magnetohydrodynamics has undergone great development during the last decades, prompted by astrophysical observations and experimental needs. At the same time, due to the astronomical scale or great energy density of such fluid bodies, turbulent flow is exceedingly common. This in turn makes magnetohydrodynamics (MHD) a very welcoming field for the study of turbulent phenomena, providing a great collection of new observations and mechanisms to further develop our intuition and ideas.

Our interest lies in the universal mechanisms of turbulence. In summary: regardless of the specific dynamics under which a fluid flows, there is some *outer scale* in which energy is introduced in the system (in the form of fluid kinetic energy) and the *Kolmogorov* or *dissipative scale* under which energy is dissipated to the medium by viscosity (or a similar effect, such as magnetic diffusivity).

The more dominant the nonlinearity of the flow is in comparison to the viscous term, the bigger is the separation of the outer and the Kolmogorov scales, forming what is called the *inertial range* over which turbulence develops. The complex behaviour of turbulent flow over this great range of scales can be said to be the core difficulty in its study; as an example, the dissipative scale of atmospheric flow is submillimetric while the outer scale spans thousands of kilometres. Completely solving the flow, in principle, demands the solution of all of the intermediate scales in the inertial range, a feat that is certainly beyond any present or foreseeable computer.

From such a brief outline, one can already point the two important questions that motivate this work:

- How is energy transferred between the scales in the inertial range?
- Is blowup (a singularity forming in finite time) possible? If so, how to describe its structure?

Our outlook is that these issues are connected. The same way as the formation of singularities in the derivatives of ocean surface waves leads to larger

dissipation [1], one expects that blowup can play an important role in the cascading of energy in the inertial range of fully developed turbulence.

The investigation of these problems demands further understanding of turbulent dynamics over a large set of scales, specially across small scales that are difficult to perceive and develop intuition about. Direct numerical simulations over such a range of scales is also prohibitive aside from the simplest cases. As an alternative, we focus on the development of blowup theory for a class of simplified models of turbulence called *shell models*. These are infinite-dimensional dynamical systems obtained after the spectral truncation of the flow equations in a way that preserves some symmetries and invariants, but allows for accurate numerical simulations.

Shell models have been found to closely emulate many turbulent phenomena, such as energy and enstrophy cascades as well as anomalies in their scaling exponents [2]. Although shell models can be regarded as toy models for turbulence, these dynamical systems are far from trivial and in the scope of this work are taken as central objects of study in their own right.

The stance of studying turbulence mechanisms from their modelling in dynamical systems naturally provides a great collection of well established techniques, such as Poincaré sections, attractors, bifurcation theory and stability theory. However, these methods are, in principle, defined for finite-dimensional systems and require that solutions exist for arbitrary time. The central achievements of this work lie in the treatment of these hurdles as we investigate solution blowup.

1.3 Modelling

1.3.1 Hydrodynamic Incompressible Flow

A flow can be identified by the specification of its velocity field $\mathbf{v} \in \mathbb{R}^3$, mass density ρ , pressure p and temperature T . Fluid dynamics has achieved great success by modeling fluids based on conservation and thermodynamic principles, namely the conservation of mass, momentum and energy and the equation of state. From these principles, one can describe the evolution of all the variables necessary to specify the state of a fluid.

In most concrete settings, it is appropriate to regard some of these variables as constants and simplify the system. For instance, a formulation in

which water or air can be regarded as incompressible is very common. In the simplest setting of fully developed turbulence, the temperature variations are decoupled from momentum and continuity equations. In this case, we are left with the *Navier-Stokes* equations for incompressible flow [3]

$$\begin{aligned}\frac{\partial \mathbf{v}}{\partial t} + \mathbf{v} \cdot \nabla \mathbf{v} &= -\nabla p + \nu \Delta \mathbf{v} + f, \\ \nabla \cdot \mathbf{v} &= 0,\end{aligned}\tag{1.1}$$

where the density ρ has been normalized to one, ν stands for the kinematic viscosity and f accounts for external forcing per unit of mass. The second equation is the incompressibility condition.

1.3.2 Magnetohydrodynamic Flow

The objects of study of Magnetohydrodynamics (MHD) are fluids susceptible to electromagnetic forces. As the fluid moves, electric charges are carried, which in turn induces change of the magnetic field. However, these fluids typically have a large number of free electrons, which can rapidly rearrange themselves in a steady state again. This simplifies the mathematical description of such a fluid, as we need only to add the induced magnetic field to the usual fluid variables to describe an MHD flow.

The unforced MHD equations for incompressible systems read [4]:

$$\begin{aligned}\frac{\partial \mathbf{v}}{\partial t} - \nu \nabla^2 \mathbf{v} &= -(\mathbf{v} \cdot \nabla) \mathbf{v} + (\mathbf{b} \cdot \nabla) \mathbf{b} - \nabla p, \\ \frac{\partial \mathbf{b}}{\partial t} - \eta \nabla^2 \mathbf{b} &= \nabla \times (\mathbf{v} \times \mathbf{b}), \\ \nabla \cdot \mathbf{v} &= 0, \quad \nabla \cdot \mathbf{b} = 0,\end{aligned}\tag{1.2}$$

where \mathbf{v} and \mathbf{b} are the velocity and induced magnetic fields, p is the total pressure, both magnetic and kinetic, while the density ρ has been taken as one. The induced magnetic field \mathbf{b} was normalized by $\sqrt{4\pi\rho}$, measured in units of velocity. These equations follow from the Navier-Stokes equation taking into account the Lorentz force and from Maxwell equations [4]. The first equation is a momentum equation considering electromagnetic forces and stress. The second equation models magnetic field dynamics, **assuming uniform conductivity. It follows from Faraday's law and Ohm's law, which**

describe eletromagetic induction and the electric current created by and electric field, respectively.

The nonlinear terms on the right-hand side redistribute magnetic and kinetic energy among the full range of scales of the system. When the transference of kinetic to magnetic energy exactly compensates energy dissipation caused by magnetic diffusivity, magnetic energy does not decay with time. This phenomenon is called dynamo action.

Three-dimensional systems have three ideal quadratic invariants, the total energy (E), the total correlation (C) and total magnetic helicity (H) given as follows:

$$\begin{aligned} E &= \frac{1}{2} \int (\mathbf{v}^2 + \mathbf{b}^2) d^3x, \\ C &= \int \mathbf{v} \cdot \mathbf{b} d^3x, \\ H &= \int \mathbf{a} \cdot (\nabla \times \mathbf{a}) d^3x, \end{aligned} \tag{1.3}$$

where $\mathbf{a} = \nabla \times \mathbf{b}$.

1.3.3 Shell Models

As we look at the balance laws working inside a fluid, first we need to determine what the distinctive characteristics are that describe the interacting parts of the fluid. The most familiar concept is the notion of spatial *scale*, having the outer and inner scales been naturally defined by the flow problem. However, how do we define the intermediate scales? We follow the usual correspondence between physical and Fourier spaces and interpret the distinction between scales as some form of filtering between subsets of wavenumbers.

Shell models arise upon analysis of one such filter, a discretization of the Fourier space onto concentric spherical shell, $k_{n-1} \leq \|\mathbf{k}\| < k_n$. The sequence $\{k_n\}_{n \in \mathbb{N}}$ is chosen as a geometric progression $k_n = k_0 h^n$, so as to significantly reduce the degrees of freedom of the model, in comparison to the full fluid equations. To each shell is assigned one or more scalar variables, which may be interpreted as some mean or projection of the spectral fluid variables onto the shell. These variables may account for fluid velocity, induced magnetic field, temperature deviation from its mean value, etc.

The spectral Navier-Stokes equation can be written as

$$\begin{aligned} \frac{\partial v_j(\mathbf{k})}{\partial t} = & -i \sum_{m,n} \int \left(\delta_{j,n} - \frac{k_j k'_n}{k^2} \right) v_m(\mathbf{k}') v_n(\mathbf{k} - \mathbf{k}') d^3 \mathbf{k}' \\ & - \nu k^2 v_j(\mathbf{k}) + f_j(\mathbf{k}). \end{aligned} \quad (1.4)$$

Following this structure, a shell model may be defined in the following functional form [2]

$$\frac{dv_n}{dt} = \mathcal{C}_n(v, v) - \mathcal{D}_n(v) + \mathcal{F}_n, \quad (1.5)$$

where $v = (v_1, v_2, \dots)$ is a vector of shell variables $v_n \in \mathbb{R}$. In this model, $\mathcal{C}_n(v, v)$ are the quadratic nonlinear coupling terms, $\mathcal{D}_n(v)$ are the linear dissipative terms and \mathcal{F}_n are the forcing terms.

A specific shell model is then constructed from (1.5) by defining the range of interaction between shells and imposing some symmetries or ideal invariants of the original flow to be preserved in the shell model. For example, assuming that shells interact only among neighbours and that energy $E = \sum v_n^2/2$ is conserved, one may write the mixed Obukhov-Novikov hydrodynamic shell model [2] as

$$\frac{dv_n}{dt} = Ak_n (v_{n-1}^2 - hv_n v_{n+1}) + Bk_n (v_{n-1} v_n - hv_{n+1}^2) - \nu k_n^2 v_n + f_n, \quad (1.6)$$

where A and B are arbitrary constants. This model is constructed over the Hilbert space ℓ^2 of the sequences $v = (v_1, v_2, \dots)$.

We note that the above construction of a shell model is quite simplistic and serves introductory purposes. There are different paths that one may tread to build shell models, such as projection of spectral flow equations onto wavelets. But we note that these different paths usually lead to the same or equivalent models if the same choices of invariances and interaction ranges have been made; this shows that the shell model construction is quite robust. For a more detailed account on shell model history and construction, we refer to [2] and [6].

1.4 Blowup

By blowup we mean the formation of singularities in finite time for some initially regular solution of an evolution model. How exactly a solution may

turn singular depends on the problem in question, but it is generally regarded as caused by the divergence of the solution or some of its derivatives as it approaches a specific blowup time t_c . After this critical point, the solution may not be well defined or may not be regarded as a solution in the classical sense.

As a first example, take an ordinary differential equation for real function $y(t)$ as

$$\frac{dy}{dt} = y^2. \quad (1.7)$$

Solutions of this equation have the form

$$y(t) = (t_c - t)^{-1}, \quad (1.8)$$

i.e., they diverge as $t \rightarrow t_c$.

Another classical example is the inviscid Burgers equation, a hyperbolic conservation law

$$\frac{\partial u}{\partial t} + u \frac{\partial u}{\partial x} = 0, \quad (1.9)$$

for a differentiable function $u(x, t)$. We can consider this equation along special curves on the plane (t, x) , called *characteristic* curves, defined under a parametrization by $s \in \mathbb{R}$ by

$$\frac{dt}{ds} = 1, \quad \frac{dx}{ds} = u. \quad (1.10)$$

For each characteristic curve, the partial differential equation (1.9) is reduced to

$$\frac{du}{ds} = \frac{\partial u}{\partial t} + u \frac{\partial u}{\partial x} = 0, \quad (1.11)$$

hence, u is constant along a characteristic. In particular, this means that characteristics are straight lines. The above construction allows to solve the Cauchy problem for given initial condition $u(0, x) = u_0(x)$ by continuation of the values $u_0(x)$ along the characteristics for $t > 0$.

According to (1.10), each characteristic has a slope $1/u_0(x)$. Thus, if there are points $x_1 < x_2$ such that

$$u_0(x_1) > u_0(x_2), \quad (1.12)$$

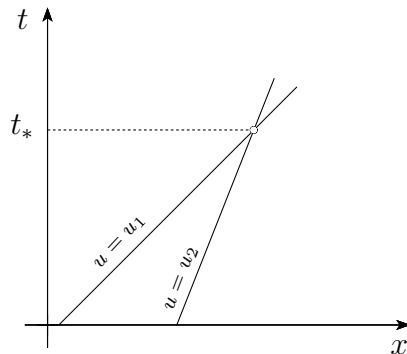


Figure 1.1: Crossing of two characteristics carrying two different solution values $u_1 = u_0(x_1)$ and $u_2 = u_0(x_2)$

then, there is some time $t_* > 0$ at which the characteristics starting at $(x_1, 0)$ and $(x_2, 0)$ cross each other, as shown in Figure 1.1. As characteristics carry different values $u_0(x_1) \neq u_0(x_2)$, the value of u at their intersection is ambiguous. This shows that a differentiable solution cannot exist for all times $t > 0$, in other words, it must blowup in finite time. The blowup of the Burgers equation leads to an infinite derivative $\partial u / \partial x$ at some point as $t \rightarrow t_c$ and then to the formation of a discontinuous (shock wave) solution, see Figure 1.2, which must be defined in a weak sense [7].

These simple examples leave a clear message: if we insist that solutions must be smooth, then we need to accept that there may be solutions which exist only for a finite time. This phenomenon is directly linked to the nonlinearity of the differential equations and is possible regardless of how smooth the initial data may be. The existence of blowup for 3D incompressible inviscid flow, as well as for the MHD flow, is an open problem [8]. Thus, shell models may provide some insight on possible blowup scenarios and help to develop methods for their analysis.

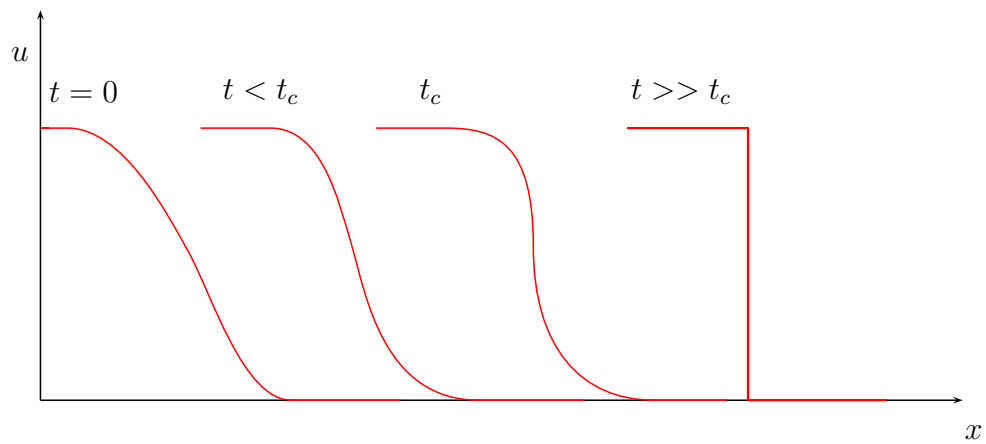


Figure 1.2: Evolution of the wave solution of the Burgers equation. As time passes, wave front is compressed as characteristic curves approach each other, resulting in a steeper slope. At the blowup time t_c , the derivative goes to infinity, resulting in a vertical slope at some point. After this blowup, solution becomes discontinuous.

Chapter 2

MHD Turbulence Shell Models and Blowup

2.1 Model

We focus our study on the shell model for MHD turbulence modified by Gloaguen *et al.* [9] from the mixed Obukhov-Novikov hydrodynamic shell model (1.6), see [10, 11]. Equations of this model read

$$\begin{aligned}\frac{dv_n}{dt} &= Ak_n[v_{n-1}^2 - b_{n-1}^2 - h(v_n v_{n+1} - b_n b_{n+1})] + \\ &\quad + Bk_n[v_{n-1}v_n - b_{n-1}b_n - h(v_{n+1}^2 - b_{n+1}^2)] - \nu k_n^2 v_n, \\ \frac{db_n}{dt} &= Ak_{n+1}[v_{n+1}b_n - v_n b_{n+1}] + Bk_n[v_n b_{n-1} - v_{n-1}b_n] - \eta k_n^2 b_n,\end{aligned}\tag{2.1}$$

where $k_n = k_0 h^n$ is a wave number, ν is the kinematic viscosity, η is the magnetic diffusivity and A and B are arbitrary coupling coefficients. Usually, one takes $h = 2$. This system is based on the restriction to real variables, v_n and b_n , which mimic the speed and magnetic field fluctuations at shell $k_n \leq |k| < k_{n+1}$ for $n = 1, 2, \dots$. Only the interaction between nearest shells is considered in this model. The system must be supplied by the initial conditions at $t = 0$ and boundary conditions for shell v_0 and b_0 , which are usually assumed to be null.

We are concerned with the uniparametric analysis of the inviscid/nondiffusive

model. Choosing $\nu = \eta = 0$, $B = 1$ and $A = \epsilon$, (2.1) is written as

$$\begin{aligned} \frac{dv_n}{dt} &= k_n[\epsilon(v_{n-1}^2 - b_{n-1}^2) + v_{n-1}v_n - b_{n-1}b_n] \\ &\quad - k_{n+1}[v_{n+1}^2 - b_{n+1}^2 + \epsilon(v_nv_{n+1} - b_nb_{n+1})], \\ \frac{db_n}{dt} &= \epsilon k_{n+1}[v_{n+1}b_n - v_nb_{n+1}] + k_n[v_nb_{n-1} - v_{n-1}b_n]. \end{aligned} \quad (2.2)$$

This model was built upon two inviscid invariants, the total energy and the cross-correlation function,

$$E = \frac{1}{2} \sum (v_n^2 + b_n^2), \quad C = \sum v_nb_n, \quad (2.3)$$

where the sum is always assumed over all shells n . These invariants mimic the energy and cross-correlation of the MHD flow, see (1.3).

2.2 Local existence of solutions and blowup

As we search for blowup in solutions of (2.2), we first need to give it a proper mathematical definition. We base our construction on something analogous to the field gradients in the shell space, defined by multiplication over the wavenumbers k_n . We choose the two norms as [12]

$$\begin{aligned} \|v'\| &= \left(\sum k_n^2 v_n^2 \right)^{1/2}, \\ \|v'\|_\infty &= \sup_n k_n |v_n|. \end{aligned} \quad (2.4)$$

In this notation, the prime signals that each shell variable is multiplied by its corresponding wavenumber, as one would have for a derivative in Fourier space. Note that the norm $\|v'\|$ is then analogous to the enstrophy in fluid dynamics. Solutions of (2.2) are called regular (or classical) if

$$\|v'\| + \|b'\| < \infty. \quad (2.5)$$

Theorem 1 *If the initial conditions at $t = 0$ satisfy the condition (2.5), there exists some $T > 0$ such that (2.2) has an unique regular solution $u(t)$ in the interval $[0, T)$.*

This theorem is based on the Picard-Lindlöf theorem for existence and unicity of initial value problems. The complete proof can be found in [13] for the Sabra shell model and its modification to other shell models is quite straightforward, as shell models in general feature the same type of bilinear coupling. We say that a solutions blows up at $t = t_c$ if it is regular at $t < t_c$ and

$$\sup_{0 \leq t < t_c} (\|v'\| + \|b'\|) = \infty. \quad (2.6)$$

The following theorem serves as a blowup criterion for model (2.2), analogous to the Beale-Kato-Majda theorem for the fluid dynamics [14].

Theorem 2 *Let $v_n(t)$ and $b_n(t)$ be a smooth solution of (2.2) satisfying the condition (2.5) for $0 \leq t < t_c$, where t_c is the maximal time of existence for such solution. Then, either $t_c = \infty$ or*

$$\int_0^{t_c} \|v'\|_\infty dt = \infty. \quad (2.7)$$

Proof: If (2.7) is satisfied for $t_c < \infty$, it follows that $\|v'\|_\infty$ is unbounded for $0 \leq t < t_c$. Hence, (2.6) is satisfied, making (2.7) a sufficient condition for blowup. Let us show that it is also a necessary condition.

Using the definitions (2.4) and equations (2.2) we find the relation

$$\begin{aligned} \frac{1}{2} \frac{d}{dt} (\|v'\|^2 + \|b'\|^2) &= \sum k_n^2 v_n \frac{dv_n}{dt} + \sum k_n^2 b_n \frac{db_n}{dt} \\ &= \sum k_n^2 v_n \{k_n [\epsilon(v_{n-1}^2 - b_{n-1}^2) + v_{n-1}v_n - b_{n-1}b_n] \\ &\quad - k_{n+1}[v_{n+1}^2 - b_{n+1}^2 + \epsilon(v_n v_{n+1} - b_n b_{n+1})]\} \\ &\quad + \sum k_n^2 b_n \{\epsilon k_{n+1}[v_{n+1}b_n - v_n b_{n+1}] + k_n[v_n b_{n-1} - v_{n-1}b_n]\}. \end{aligned} \quad (2.8)$$

The right-hand side of the above expression can be written as a sum of series. Inside each series, one can use the bound $k_n |v_n| \leq \|v'\|_\infty$ for any shell number n , as well as the Cauchy-Schwarz inequality where necessary, as in the example

$$\begin{aligned} \left| \sum k_n^3 v_n b_{n-1} b_n \right| &\leq \|v'\|_\infty h \sum (k_{n-1} b_{n-1})(k_n b_n) \\ &\leq \|v'\|_\infty h \left(\sum k_{n-1}^2 b_{n-1}^2 \right)^{1/2} \left(\sum k_n^2 b_n^2 \right)^{1/2} \\ &\leq h \|v'\|_\infty \|b'\|^2, \end{aligned}$$

where we used $k_n = hk_{n-1}$. Performing similar estimates for each series, we find some positive constant D for which

$$\frac{d}{dt} \left(\|v'\|^2 + \|b'\|^2 \right) < D \|v'\|_\infty \left(\|v'\|^2 + \|b'\|^2 \right). \quad (2.9)$$

From the use of the Grownwall inequality we can find an upper bound for the sum of the squared norms:

$$\left(\|v'\|^2 + \|b'\|^2 \right)_{t=t_c} \leq \left(\|v'\|^2 + \|b'\|^2 \right)_{t=0} \exp \left(D \int_0^{t_c} \|v'\|_\infty dt \right). \quad (2.10)$$

This relation proves that (2.7) is necessary for (2.6). \square

Theorem 2 states that blowup is necessarily associated with unbounded values of $k_n v_n$, which by analogy with fluid dynamics can be interpreted as a blowup in vorticity.

We note that the existence of solutions in a weak sense can be proven after blowup, $t > t_c$, as for the Sabra shell model [13]. However, such a proof does not guaranties its uniqueness. In fact, one can show that an infinite number of solutions appear after blowup [15].

Chapter 3

Renormalization and Symmetry

3.1 Renormalization Scheme

Our objective here is to write the shell model equations (2.2) under new renormalized variables so that the blowup time t_c is taken to infinity, enabling the use of dynamical system methods. This is accomplished by an analogous scheme to the one proposed by Dombre and Gilson [16] for the mixed Obukhov-Novikov model [10, 11] and by Mailybaev for a convective turbulence shell model [12].

We introduce the renormalized time τ defined implicitly by

$$t = \int_0^\tau \exp\left(-\int_0^{\tau'} R(\tau'') d\tau''\right) d\tau', \quad (3.1)$$

where the function $R(\tau)$ is specified later in (3.6). The renormalized shell speed u_n and renormalized induced shell magnetic field β_n are defined as

$$\begin{aligned} u_n &= \exp\left(-\int_0^\tau R(\tau') d\tau'\right) k_n v_n, \\ \beta_n &= \exp\left(-\int_0^\tau R(\tau') d\tau'\right) k_n b_n. \end{aligned} \quad (3.2)$$

The system of equations that describe the temporal evolution of the renormalized model can be easily obtained by differentiating (3.2) with respect to τ , using the definition of $t(\tau)$ given by (3.1) and the original system (2.2). Our renormalized model is thus given by:

$$\frac{du_n}{d\tau} = -Ru_n + P_n, \quad \frac{d\beta_n}{d\tau} = -R\beta_n + Q_n \quad (3.3)$$

where

$$\begin{aligned}
P_n &= \epsilon(h^2(u_{n-1}^2 - \beta_{n-1}^2) - u_n u_{n+1} + \beta_n \beta_{n+1}) \\
&\quad + h(u_{n-1} u_n - \beta_{n-1} \beta_n) - h^{-1}(u_{n+1}^2 - \beta_{n+1}^2), \\
Q_n &= \epsilon(u_{n+1} \beta_n - u_n \beta_{n+1}) + h(u_n \beta_{n-1} - u_{n-1} \beta_n).
\end{aligned} \tag{3.4}$$

The function $R(\tau)$ is determined by imposing an invariant over the renormalized system (3.3). Namely, we want to conserve the sum $\sum (u_n^2 + \beta_n^2)$. Then

$$\frac{1}{2} \frac{d}{d\tau} \sum (u_n^2 + \beta_n^2) = \sum (u_n P_n + \beta_n Q_n) - R \sum (u_n^2 + \beta_n^2) = 0 \tag{3.5}$$

is satisfied if

$$R = \frac{\sum (u_n P_n + \beta_n Q_n)}{\sum (u_n^2 + \beta_n^2)}. \tag{3.6}$$

This defines the missing function R in terms of model variables.

Using norm definition (2.4) and expressions (3.2), we have at $t = \tau = 0$,

$$\sum u_n^2 = \sum k_n^2 v_n^2 = \|v'\|^2, \quad \sum \beta_n^2 = \sum k_n^2 b_n^2 = \|b'\|^2. \tag{3.7}$$

Hence, the regularity condition implies that $\sum (u_n^2 + \beta_n^2) < \infty$. Thus, we say that a solution $u_n(\tau), \beta_n(\tau)$ is regular if it has finite ℓ^2 -norm.

Now we verify that our renormalized shell model is well defined globally in time for any regular initial condition.

Lemma 3 *For any nontrivial initial conditions of finite ℓ^2 -norm, a regular solution u_n and β_n of the renormalized system (3.3) exists and is unique for $0 \leq \tau < \infty$. This solution is related by (3.1) and (3.2) to the regular solution v_n and b_n of the original system (2.2) for $t < t_c$, where $t_c = \lim_{\tau \rightarrow \infty} t(\tau)$.*

Proof: Since we have constructed the renormalized system (3.3) from system (2.2) by defining (3.2), it suffices only to show that (3.6) is well defined and that any $\tau \geq 0$ corresponds to $t < t_c$.

As the norm $C = \sum (u_n^2 + \beta_n^2) < \infty$ is conserved, it follows that $|u_n| \leq C^{1/2}$ and $|\beta_n| \leq C^{1/2}$. Since the denominator in (3.6) is equal to constant C , we need only consider the numerator in the definition of $R(\tau)$. Substitution of P_n and Q_n given by (3.4) leads to

$$\begin{aligned}
\sum (u_n P_n + \beta_n Q_n) &= \sum u_n [\epsilon(h^2(u_{n-1}^2 - \beta_{n-1}^2) - u_n u_{n+1} + \beta_n \beta_{n+1}) \\
&\quad + h(u_{n-1} u_n - \beta_{n-1} \beta_n) - h^{-1}(u_{n+1}^2 - \beta_{n+1}^2)] \\
&\quad + \sum \beta_n [\epsilon(u_{n+1} \beta_n - u_n \beta_{n+1}) + h(u_n \beta_{n-1} - u_{n-1} \beta_n)].
\end{aligned}$$

Every term in the right-and side can be bounded as, for example, the first term

$$\begin{aligned} \left| \sum u_n \epsilon h^2 u_{n-1}^2 \right| &\leq |\epsilon| h^2 C^{1/2} \sum |u_{n-1}^2| \\ &\leq |\epsilon| h^2 C^{3/2}. \end{aligned} \quad (3.8)$$

As such, the function $R(\tau)$ is bounded for all $\tau \geq 0$.

From the definitions (3.2) and the condition $|u_n| \leq C^{1/2}$ we have, for $t(\tau)$ given by (3.1),

$$|k_n v_n(t)| \leq C^{1/2} \exp \left(\int_0^\tau R(\tau') d\tau' \right), \quad (3.9)$$

i.e. $\|v'\|_\infty < \infty$ for any τ . By Theorem 2 we have that this solution cannot blowup for any $t(\tau) < t_c$, where $t_c = \lim_{\tau \rightarrow \infty} t(\tau)$. Then, Theorem 1 implies the existence and uniqueness of solution $v_n(t)$, $b_n(t)$ for every such $t(\tau)$. Relations (3.1) and (3.2) map these solutions of (2.2) into unique solutions $u_n(\tau)$ and $\beta_n(\tau)$ of (3.3) which exist globally in τ . \square

3.2 Symmetry

In this section, we describe symmetries of the shell model which were found useful for further study. It is straightforward to see that the renormalized system (3.3), (3.4) and (3.6) has the following symmetries:

(S.R.1) $\tau \rightarrow \tau/a$, $u_n \rightarrow au_n$, $\beta_n \rightarrow a\beta_n$ for arbitrary real constant a ;

(S.R.2) $\tau \rightarrow \tau - \tau_0$ for arbitrary real constant τ_0 ;

(S.R.3) $u_n \rightarrow u_{n+1}$, $\beta_n \rightarrow \beta_{n+1}$.

Note that symmetry (S.R.3) does not hold at the left boundary, as our model was initially defined only for $n \in \mathbb{N}$.

Lemma 4 *The definitions (3.1) and (3.2) relate symmetries (S.R.1)-(S.R.3) of the renormalized system (3.3) to the following symmetries of the original system (2.2):*

(S.N.1) $t \rightarrow t/a$, $v_n \rightarrow av_n$, $b_n \rightarrow ab_n$ for arbitrary real constant a ;

(S.N.2) $t \rightarrow (t - t_0)/a$, $v_n \rightarrow av_n$, $b_n \rightarrow ab_n$, where both a and t_0 are constants uniquely determined by τ_0 in (S.R.2) and the corresponding solution u_n, β_n ;

(S.N.3) $v_n \rightarrow hv_{n+1}$, $b_n \rightarrow hb_{n+1}$.

Proof: Here we prove only symmetry (S.N.2), which is the most complicated. The other symmetries are proven with similar arguments. Let $\hat{\tau} = \tau - \tau_0$, and consider new solutions (denoted with a hat) that are obtained by the time shift as $\hat{u}_n(\hat{\tau}) = u_n(\tau)$, $\hat{\beta}_n(\hat{\tau}) = \beta_n(\tau)$. It follows from (3.6) that $\hat{R}(\hat{\tau}) = R(\tau) = R(\hat{\tau} + \tau_0)$. From definition (3.1):

$$\begin{aligned} \hat{t} &= \int_0^{\hat{\tau}} \exp\left(-\int_0^{\tau'} \hat{R}(\hat{\tau}'') d\tau''\right) d\tau' = \int_0^{\tau-\tau_0} \exp\left(-\int_0^{\tau'} R(\tau'' + \tau_0) d\tau''\right) d\tau' \\ &= \int_{\tau_0}^{\tau} \exp\left(-\int_{\tau_0}^{\xi'} R(\xi'') d\xi''\right) d\xi', \end{aligned} \quad (3.10)$$

where we have made the substitutions $\xi' = \tau' + \tau_0$ and $\xi'' = \tau'' + \tau_0$. Note that

$$\exp\left(-\int_{\tau_0}^{\xi'} R(\xi'') d\xi''\right) = \exp\left(-\int_0^{\xi'} R(\xi'') d\xi''\right) \exp\left(\int_0^{\tau_0} R(\xi'') d\xi''\right). \quad (3.11)$$

Then, expression (3.10) yields $\hat{t} = (t - t_0)/a$, where

$$a = \exp\left(-\int_0^{\tau_0} R(\tau'') d\tau''\right), \quad t_0 = \int_0^{\tau_0} \exp\left(-\int_0^{\tau'} R(\tau'') d\tau''\right) d\tau'. \quad (3.12)$$

Note that constants a and t_0 depend not only on τ_0 but also on the associated renormalized system solution u_n and β_n through (3.6). In a similar manner, using (3.2) we have

$$\begin{aligned} \hat{v}_n(\hat{t}) &= \exp\left(\int_0^{\hat{\tau}} \hat{R}(\tau') d\tau'\right) k_n^{-1} \hat{u}_n(\hat{\tau}) = \exp\left(\int_0^{\tau-\tau_0} R(\tau' + \tau_0) d\tau'\right) k_n^{-1} u_n(\tau) \\ &= \exp\left(\int_{\tau_0}^{\tau} R(\xi') d\xi'\right) k_n^{-1} u_n(\tau) = av_n(t). \end{aligned} \quad (3.13)$$

Symmetry for $b_n(t)$ follows in exactly the same way. \square

Chapter 4

Asymptotic Blowup Solution of a Hydrodynamic Model

For vanishing magnetic field variables, $b_n \equiv 0$, system (2.2) reduces to the mixed Obukhov-Novikov shell model for hydrodynamic turbulence [10,11]

$$\frac{dv_n}{dt} = k_n[\epsilon(v_{n-1}^2 - hv_nv_{n+1}) + v_{n-1}v_n - hv_{n+1}^2], \quad (4.1)$$

which is associated by definitions (3.1) and (3.2) to the renormalized system:

$$\begin{aligned} \frac{du_n}{d\tau} &= -R(\tau)u_n + P_n, \\ R(\tau) &= \frac{\sum u_n P_n}{\sum u_n^2}, \\ P_n &= \epsilon(h^2 u_{n-1}^2 - u_n u_{n+1}) + hu_{n-1}u_n - h^{-1}u_{n+1}^2. \end{aligned} \quad (4.2)$$

The blowup problem for model (4.1) was studied in [16]. In this chapter, we reproduce these results in order to facilitate the blowup study for the MHD shell model.

4.1 Numerical simulation

For the numerical integration of our models we used the Runge-Kutta-Fehlberg method, natively implemented in MATLAB. Throughout this work we have kept the choice of parameters most used in the literature, $k_0 = 1$ and $h = 2$. Only the first three shells were provided with nonzero initial conditions. We

truncated the shell model at the hundredth shell. Such a system is long enough for the initial perturbation to propagate to an asymptotic solution.

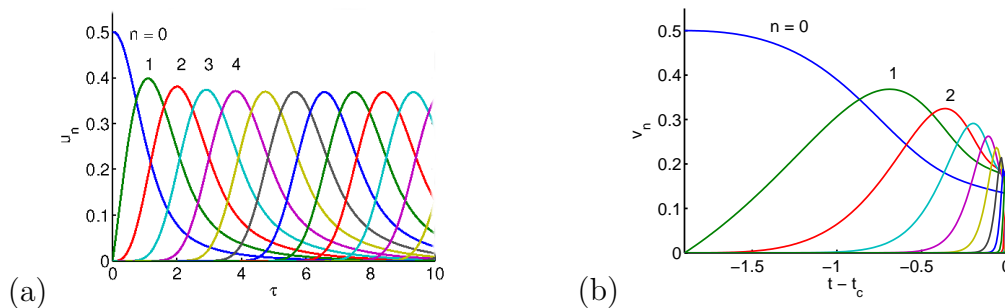


Figure 4.1: Blowup for the inviscid O.N. hydrodynamic shell model for $\epsilon = 0.5$: (a) a travelling wave for renormalized variable $u_n(\tau)$; (b) numerical solution for variable $v_n(t)$. The blowup time $t_c = 1.89$ corresponds to $\tau \rightarrow \infty$.

For ϵ between $[-10, -1]$ and $[0.5, 10]$ numerical simulations yield travelling wave solutions for (4.2) at large enough renormalized time τ . These asymptotic solutions were first observed in [16]. Such travelling waves have the form

$$u_n(\tau) = aU(n - a\tau), \quad (4.3)$$

i.e., the wave travels towards larger n with constant positive speed a . Function $U(\xi) \rightarrow 0$ as $\xi \rightarrow \pm\infty$. Note that a in (4.3) is related to symmetry (S.R.1)

$$\tau \mapsto \frac{\tau}{a}, \quad u_n \mapsto au_n \quad (4.4)$$

Thus, with no loss of generality, we can take $a = 1$ in further analysis.

Figure 4.1 (a) shows an example of the aforementioned travelling wave solution. As one can observe, the convergence to a self-similar solution of the form (4.3) is quite fast: for $n \geq 3$ the renormalized shell variables $u_n(\tau)$ follow the same pattern given by the function $U(\xi)$ in (4.3). In Figure 4.1 (b) we present the numerical solution of system (4.1) for the same values of parameters and initial values equivalent (by (3.2)) to the ones used in the previous figure. Successive shell variables $v_n(t)$ are similar upon some rescaling. Such a rescaling should take into account how the shell velocities are compressed in their amplitude and in time as they approach blowup time. Comparison of Figures 4.1 (a) and 4.1 (b) shows that, having taken the

blowup time to infinity by renormalization scheme (3.1) and (3.2), travelling wave solutions $u_n(\tau)$ of the renormalized system (3.3) induces a self-similar blowup.

4.2 Asymptotic Blowup Solution

The following result, obtained in [16], provides a rigorous explanation to this fact; it gives self-similar solutions for the original variables $v_n(t)$ based on the solutions found for the renormalized variables $u_n(\tau)$. We provide the detailed proof following [12].

Theorem 5 *Taking $a = 1$ in (4.3), let us define the scaling exponent*

$$y = \frac{1}{\log h} \int_0^1 R(\tau) d\tau \quad (4.5)$$

and the function

$$V(t - t_c) = \exp\left(\int_0^\tau R(\tau) d\tau\right) U(-\tau), \quad (4.6)$$

where τ is related to t by (3.1) and $R(\tau)$ is given by (4.2).

If $y > 0$, then the solution $v_n(t)$ associated with (4.3) is given by

$$v_n(t) = k_n^{y-1} V(k_n^y(t - t_c)). \quad (4.7)$$

This solution blows up at finite time

$$t_c = \int_0^\infty \exp\left(-\int_0^{\tau'} R(\tau'') d\tau''\right) d\tau'. \quad (4.8)$$

Proof: First, let us show that integral (4.8) converges. From (4.3) and (4.2), we conclude that $R(\tau)$ must be periodic with period $1/a = 1$. As such, from definition (4.5), a constant D can be found satisfying the inequality

$$\int_0^\tau R(\tau') d\tau' > D + \tau y \log h \quad (4.9)$$

Using this inequality in the definition of t_c in (4.8), one attains the desired result for every positive y

$$t_c < \int_0^\infty \exp(-D - \tau y \log h) d\tau < \infty.$$

Starting from the definition of y in (4.5) and using $k_n = h^n$ as well as the periodicity of $R(\tau)$, it is easy to verify that, for all positive τ ,

$$k_n^y = \exp\left(\int_{\tau}^{\tau+n} R(\tau')d\tau'\right). \quad (4.10)$$

Let us study time t' correspondent to $\tau + n$. Using definitions (3.1), (4.8) and the change of variables $\tau' = \hat{\tau} + n$,

$$\begin{aligned} t_c - t' &= \int_{\tau+n}^{\infty} \exp\left(-\int_0^{\tau'} R(\tau'')d\tau''\right) d\tau' = \int_{\tau}^{\infty} \exp\left(-\int_0^{\hat{\tau}+n} R(\tau'')d\tau''\right) d\hat{\tau} \\ &= \int_{\tau}^{\infty} \exp\left(-\int_0^{\hat{\tau}} R(\tau'')d\tau'' - \int_{\hat{\tau}}^{\hat{\tau}+n} R(\tau'')d\tau''\right) d\hat{\tau}. \end{aligned} \quad (4.11)$$

Comparing with (4.10), we arrive at

$$t_c - t' = k_n^{-y}(t_c - t). \quad (4.12)$$

Similarly, using (3.2), (4.10), (4.3) and definition (4.6)

$$\begin{aligned} v_n(t') &= k_n^{-1} \exp\left(\int_0^{\tau+n} R(\tau')d\tau'\right) u_n(\tau + n) \\ &= k_n^{y-1} \exp\left(\int_0^{\tau} R(\tau')d\tau'\right) U(-\tau) = k_n^{y-1} V(t - t_c) \end{aligned} \quad (4.13)$$

Substituting (4.12) into (4.13), we obtain the identity (4.7). Expression (4.9) also implies that

$$\exp\left(\int_0^{\tau} R(\tau')d\tau'\right) \rightarrow \infty \quad \text{as } \tau \rightarrow \infty. \quad (4.14)$$

According to (3.2) and (4.3), this yields an unbounded norm $\|v'\|_{\infty}$ for $t \rightarrow t_c^-$, i.e., the solution indeed blows up at $t = t_c$. \square

Note that the function $V(\xi)$ and the scaling exponent y do not depend on initial conditions. In this regard, the asymptotic solution of the form (4.7) can be said to be universal. Using symmetry (*S.R.1*), one can write the asymptotic formula (4.7) for any wave speed a as

$$v_n(t) = ak_n^{y-1} V(ak_n^y(t - t_c)). \quad (4.15)$$

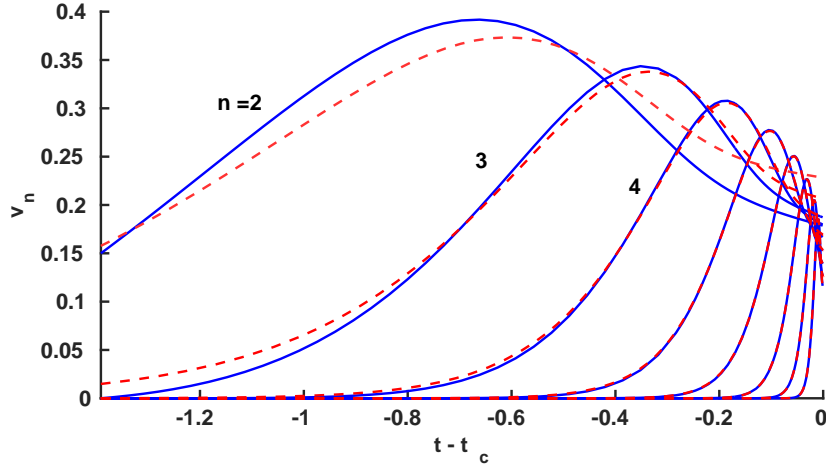


Figure 4.2: Numerical (solid blue) and asymptotic self-similar (dashed red) solutions of (4.1) near blowup.

Using the same parameters and initial conditions as in Figure 4.1, we compute the asymptotic solution (4.15) near the blowup based on Theorem 5. This solution is presented by dashed lines in Figure 4.2. We observe that the solution of the shell model (4.1), shown in Figure 4.2 by solid lines, indeed tends to a self-similar form near blowup, as we proved in Theorem 5. A very good agreement between the solutions is already achieved at the fourth shell.

Chapter 5

Attractors

From the previous analysis of the Obukhov-Novikov hydrodynamic shell model (4.1) for $\epsilon = 0.5$, we saw how the blowup structure of a shell model can be characterized in terms of a limiting solution of the corresponding renormalized model, namely its travelling wave solution. However, this type of solution does not exist for every value of ϵ . Periodic and chaotically pulsating waves also appear as limiting solutions of the renormalized system (3.3). We now develop a broader framework for these limiting solutions in terms of attractors of a Poincaré map.

5.1 Poincaré Maps

We consider the infinite dimensional Hilbert space W composed by the renormalized shell variables

$$w = (\dots, u_{n-1}, u_n, u_{n+1}, \dots, \beta_{n-1}, \beta_n, \beta_{n+1}, \dots) \in W, \quad (5.1)$$

equipped with the ℓ^2 norm $\|w\|^2 = \sum (u_n^2 + \beta_n^2)$. From Lemma 3, if $\|w(0)\| < \infty$ we conclude that $w(\tau) \in W$ for $\tau \geq 0$. Since blowup is associated with large shell numbers n , it is convenient to relax the boundary condition at $n = 0$, considering a model for $n \in \mathbb{Z}$ shell numbers, and to thoroughly use the symmetry (S.R.3) of shell number shift.

We define a real shell number n_w for the center of the solution "wave packet" to be

$$n_w(\tau) = \frac{\sum n (u_n^2(\tau) + \beta_n^2(\tau))}{\sum (u_n^2(\tau) + \beta_n^2(\tau))}. \quad (5.2)$$

Recall that the denominator of (5.2) is constant, see Section 3.1.

We define a sequence of real times $\{\tau_i\}_{i \in \mathbb{Z}}$ such that

$$n_w(\tau_i) = n_w(0) + i, \quad (5.3)$$

where $\tau_0 = 0$ and $\tau_i > 0$ is the minimum value satisfying the above relation (assuming that such time exists). The transfer operator between these times may be defined by

$$w(\tau_{i+1}) = \mathcal{T}w(\tau_i). \quad (5.4)$$

The operator \mathcal{T} is well defined for a given w as long as the center n_w of the solution travels by 1 with the increase of τ . Numerical computations lead us to believe that, for any nontrivial $w(0) \in W$, $n_w \rightarrow \infty$ as $\tau \rightarrow \infty$. In this case, the transfer operator \mathcal{T} should be well defined for any nontrivial initial condition.

In addition, we define the operator \mathcal{S} , which shifts a state vector w by one shell number to the left, as

$$w' = \mathcal{S}w, \quad u'_n = u_{n+1}, \quad \beta'_n = \beta_{n+1}. \quad (5.5)$$

The action of the operators \mathcal{T} and \mathcal{S} is illustrated in Figure 5.1.

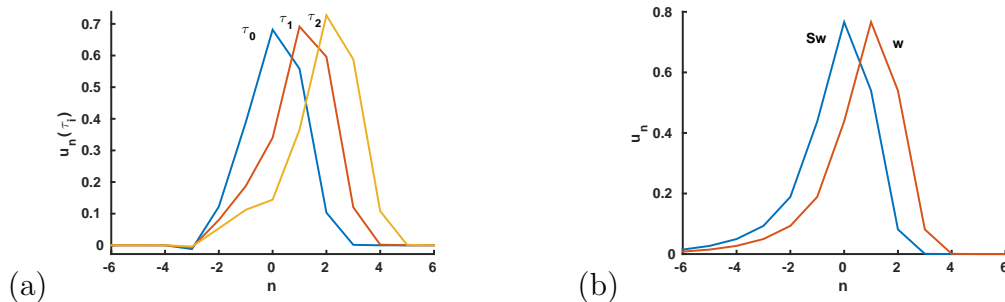


Figure 5.1: Plot of shell velocities versus shell numbers of the inviscid O.N. hydrodynamic shell model for $\epsilon = 0.5$: (a) actions of the transfer operators $\mathcal{T} : w(\tau_0) \mapsto w(\tau_1)$ and $\mathcal{T}^2 : w(\tau_0) \mapsto w(\tau_2)$; (b) action of the shift operator \mathcal{S} .

We may now define the Poincaré map as $\mathcal{P} = \mathcal{S}\mathcal{T}$

$$w' = \mathcal{P}w(0), \quad u'_n = u_{n+1}(\tau_1), \quad \beta'_n = \beta_{n+1}(\tau_1). \quad (5.6)$$

In such a case, one can see that its iterates are given by

$$\mathcal{P}^i = (\mathcal{S}\mathcal{T})^i = \mathcal{S}^i\mathcal{T}^i, \quad (5.7)$$

having used that \mathcal{T} commutes with \mathcal{S} because the renormalized system is translation invariant. Then, the iterate of the Poincaré map is written as

$$w' = \mathcal{P}^i w(0), \quad u'_n = u_{n+i}(\tau_i), \quad \beta'_n = \beta_{n+i}(\tau_i). \quad (5.8)$$

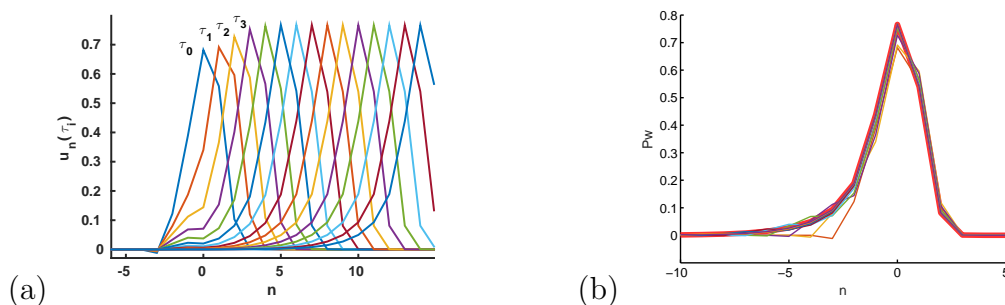


Figure 5.2: Plot of shell velocities versus shell numbers of the inviscid O.N. hydrodynamic shell model for $\epsilon = 0.5$: (a) discrete dynamics induced by the transfer operator \mathcal{T} ; (b) Poincaré map iterates \mathcal{P}^i for $i = 0, \dots, 5$ and its attractor (bold line).

As one can observe by comparing Figures 5.2, iterating the Poincaré map $\mathcal{P} = \mathcal{S}\mathcal{T}$ to an initial condition $w(0)$ equates to following the system dynamics in the moving frame along the logarithmic axis $n = \log_h k_n$ in the Fourier space. Indeed, the evolution by one shell number with \mathcal{T} is compensated with a shift \mathcal{S} by one shell number in the opposite direction. In the previous sections, we saw how asymptotic blowup solution (4.15) corresponds to a travelling solution of the renormalized system. This limiting solution is a fixed point attractor of the Poincaré map, shown by the bold line in Figure 5.2 (b). In this case, we achieve a good agreement between the iterates of the Poincaré map and its fixed-point in about five iterations.

5.2 Attractors

Shell models of turbulence present rich dynamics which have yet to be completely understood. Not only can one observe fixed-point attractor for the Poincaré map (5.6) of the renormalized system, but also periodic, quasi-periodic and chaotic attractors. The type of dynamics depends on the choice of model parameters. A detailed account to the attractor variety in a convective shell model may be found in [12].

Our renormalized MHD shell model (3.3) presents three types of attractors for the Poincaré map: fixed-point, periodic and chaotic attractors. Each of these attractors corresponds to travelling, periodically pulsating and chaotically pulsating waves, respectively.

We numerically iterate the Poincaré map (5.8) using a MATLAB native solver based on the Runge-Kutta-Fehlberg method (ode45 function), coupled with its event location capability to detect when the solution center travels integer distances in the logarithmic (shell number) axis (5.3). For initial conditions, we take nonzero values only at two neighbouring shells.

We now present a set of numerical solutions which exemplify different types of attractors found in our renormalized model. We compare the discrete dynamics of the Poincaré map and its attractors to the different types of corresponding wave solutions.

We note that the renormalized hydrodynamic model (4.2) is equivalent to the renormalized MHD model (3.3), when one sets the magnetic field variables to zero. Thus, Figure 5.2 depicts the MHD shell model dynamics with vanishing magnetic field.

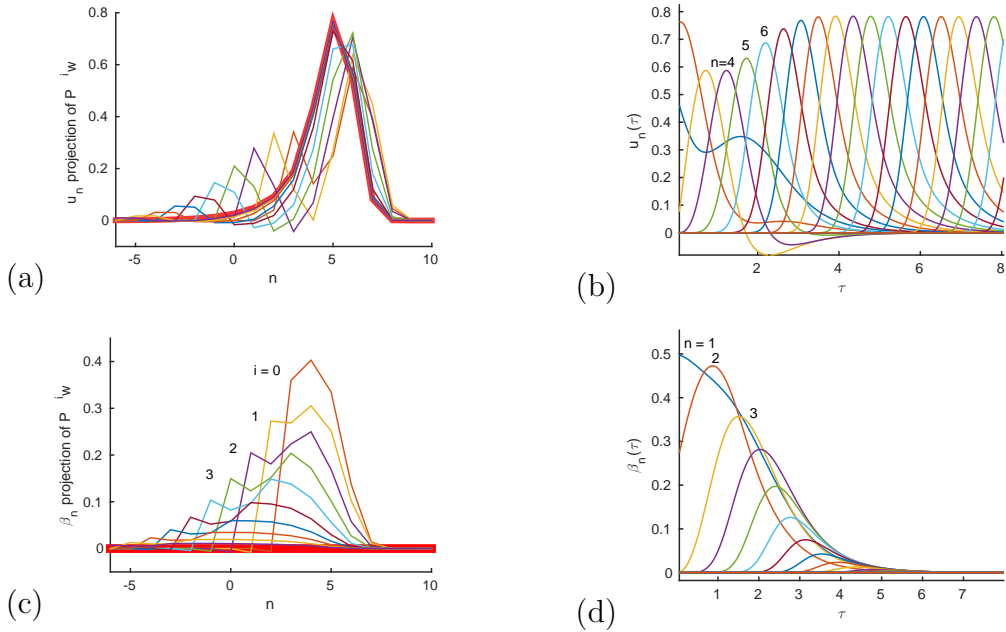


Figure 5.3: Numerical solution of inviscid/nondiffusive renormalized MHD shell model for $\epsilon = 0.5$. (a) and (c) show renormalized shell velocities and magnetic field after Poincaré map iterations; bold red lines correspond to their attractors. (b) and (d) show the corresponding travelling wave solutions for u_n and β_n .

Figure 5.3 shows the same attractor for the MHD model as previously observed in Figure 5.2, this time developed from a nontrivial initial condition for the renormalized magnetic field variables β_n . From our numerical solutions, we see that the renormalized magnetic field tends to disappear for large renormalized times τ . This serves as an example when only the shell velocity variables are responsible for the development of blowup.

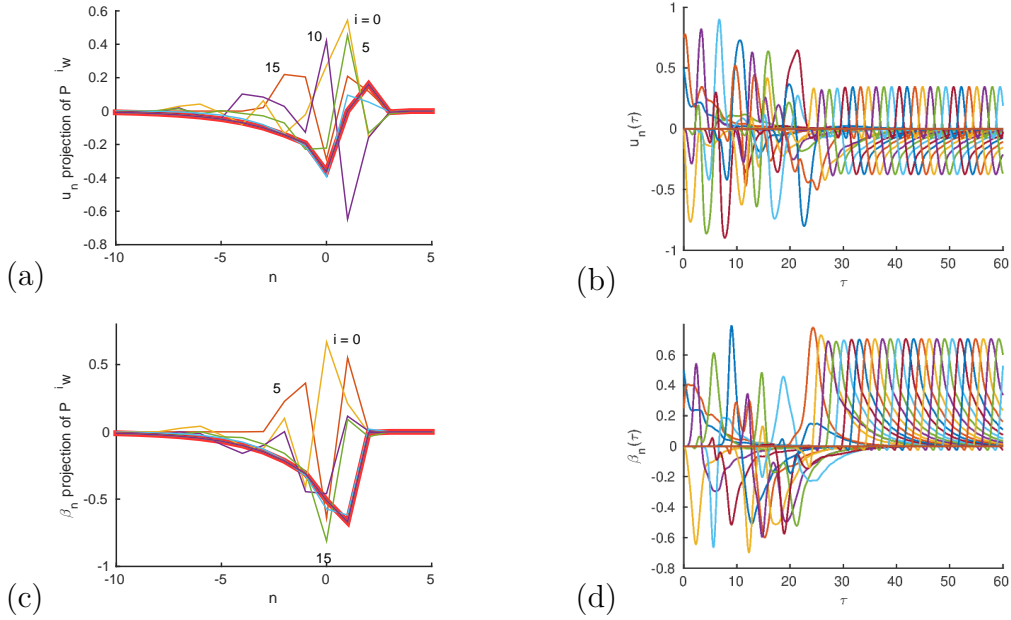


Figure 5.4: Numerical solution of inviscid/nondiffusive renormalized MHD shell model for $\epsilon = -0.35$. (a) and (c) show renormalized shell velocities and magnetic field after Poincaré map iterations; bold red lines correspond to their attractors. (b) and (d) show the corresponding travelling wave solutions for u_n and β_n .

Figure 5.4 presents an example of fixed-point attractor which is not a purely hydrodynamic solution. It represents an equilibrium between the kinetic and magnetic components in a travelling wave, unlike the previous case (Figure 5.3) when only the kinetic component survives. Even a very small presence of magnetic field in the initial conditions yields a blowup driven jointly by the velocity and magnetic fields. This magnetic field induction may be interpreted as analogous to the dynamo effect, a central open problem in MHD turbulence with great application interest. Namely, the generation and stability of magnetic fields in celestial bodies and thermonuclear fusion reactors.

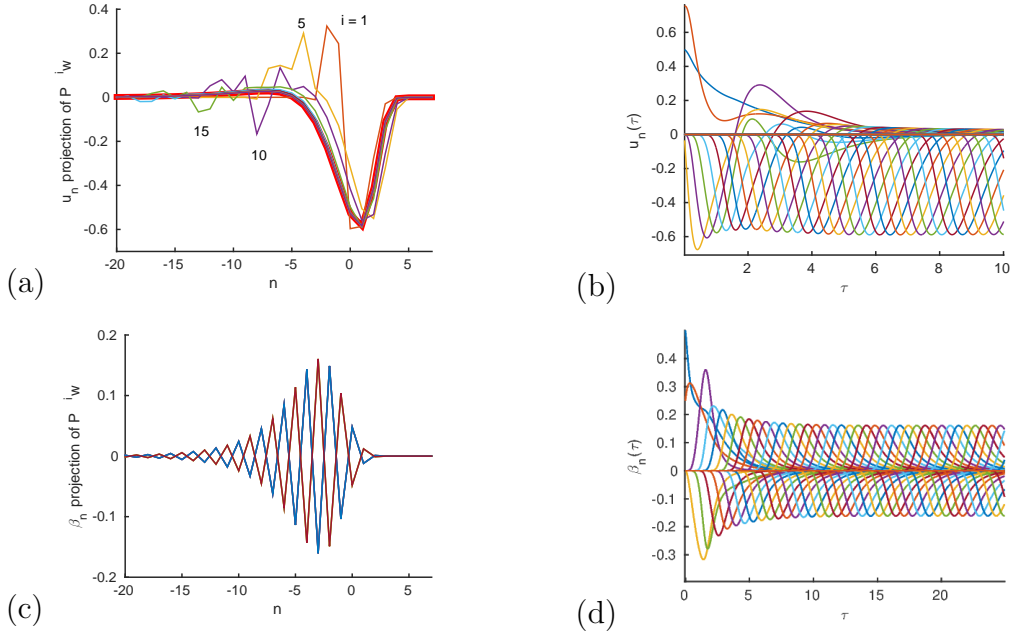


Figure 5.5: Numerical solution of inviscid/nondiffusive renormalized MHD shell model for $\epsilon = -1.3$. (a) and (c) show renormalized shell velocities and magnetic field after Poincaré map iterations; (b) and (d) show the corresponding travelling wave solutions for u_n and β_n . (c) is formed by plots of a hundred consecutive iterates of the Poincaré map, for $i > 500$, which are superimposed due to their convergence.

Figures 5.5 show the attractor of the Poincaré map (5.6) may present different periods for the u_n and β_n variables. In this case, the velocity component develops a fixed-point attractor, while in the magnetic component a period-2 attractor emerges. In this case, two consecutive shell magnetic variables are symmetric under its change of sign, as seen in Figures 5.5 (c) and (d).

We observe chaotically pulsating waves in Figure 5.6 (b) and (d), whose amplitudes are bounded by some envelopes. This bounding can be perceived in Figures 5.6 (a) and (c), which present a hundred consecutive iterations of the Poincaré map, ignoring the first thousand to eliminate transiency.

The type of an attractor may be readily seen using their projections on

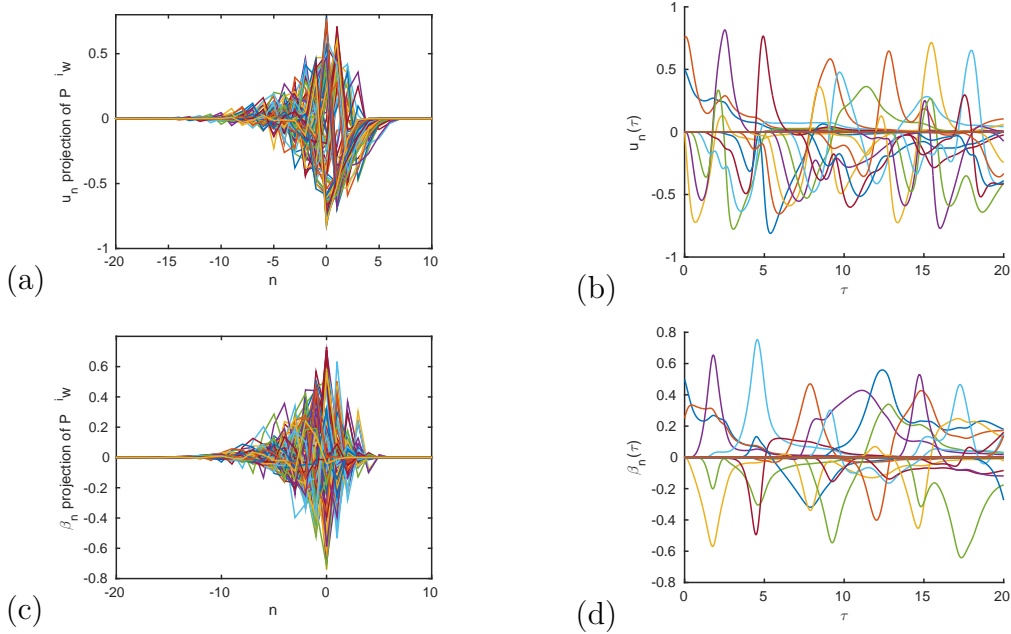


Figure 5.6: Numerical solution of inviscid/nondiffusive renormalized MHD shell model for $\epsilon = -0.8$. (a) and (c) show renormalized shell velocities and magnetic field after Poincaré map iterations; (b) and (d) show the corresponding chaotic wave solutions for u_n and β_n .

planes (u_n, β_n) , for some fixed n . This method, aside from visually appealing, is a useful test to distinguish quasi-periodic attractors from chaotic ones, as the former would present closed contours, while the latter yields a fractal set. Quasi-periodic attractors were observed in [12] for a shell model of convective turbulence, but have not been found for the MHD model (3.3). The projections of a Poincaré section onto a single pair of shell variables (u_{70}, β_{70}) are shown in Figure 5.7. In both pictures, the first thousand iterates of the Poincaré map were ignored to eliminate transient effects. Figure 5.7 (a) shows this section in the case of a period-2 attractor, depicting two periodic fixed points. Figure 5.7 (b) shows this Poincaré section in the case of a chaotic attractor, characterized by a cloud of scattered points (u_{70}, β_{70}) bound in a region of the phase space.

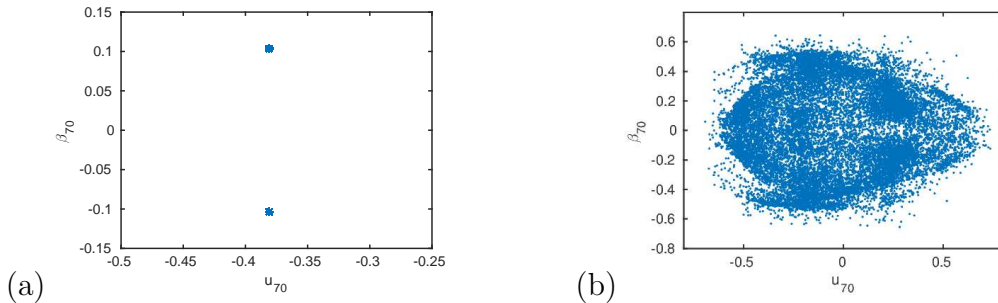


Figure 5.7: Attractors on the plane (u_n, β_n) for $n_w = 70$, (a) periodic for $\epsilon = -1.3$; (b) chaotic for $\epsilon = -0.8$.

5.3 Bifurcation Diagrams

In our approach, it is important to identify the type of attractor of (3.3) for a corresponding parameter value. For this purpose, a bifurcation diagram is very useful. We numerically construct it by computing the iterates of the Poincaré map the same way as done for the attractors above, but this time over a large set of values for the parameter ϵ . For visualization, it is convenient to take the projection of these iterates at a single shell. Naturally, a shell $n \approx n_w$ near the center of the renormalized solution is chosen. The resulting bifurcation diagram was obtained numerically through parallel computations in MATLAB and may be observed in Figure 5.8.

For $\epsilon < -1.5$ or $\epsilon > 0.5$ (not shown in the figure), we have only observed fixed-point attractors. In both figures we notice various bifurcations with a fast transition to chaos. As one would expect, chaotic behaviour is always simultaneous between the kinetic and magnetic components.

Between the two big chaotic windows, the interval $[-0.4, -0.25]$ presents an interesting mix of behaviours; not only is it composed of fixed-point and periodic attractors, it also has a very small chaotic parameter interval. Moreover, this interval is unique in a few senses. It is the only set of parameters for which nonzero fixed point attractors develop for the magnetic field; it is also the set over which sign inversion symmetry of the magnetic field is broken. All these peculiarities prompted a more detailed study of this interval. We then computed new bifurcation diagrams over this interval, this time using a continuation algorithm: we take the last iterate from the attractor of the previous parameter as the initial condition to compute the attractor for a new neighbouring parameter.

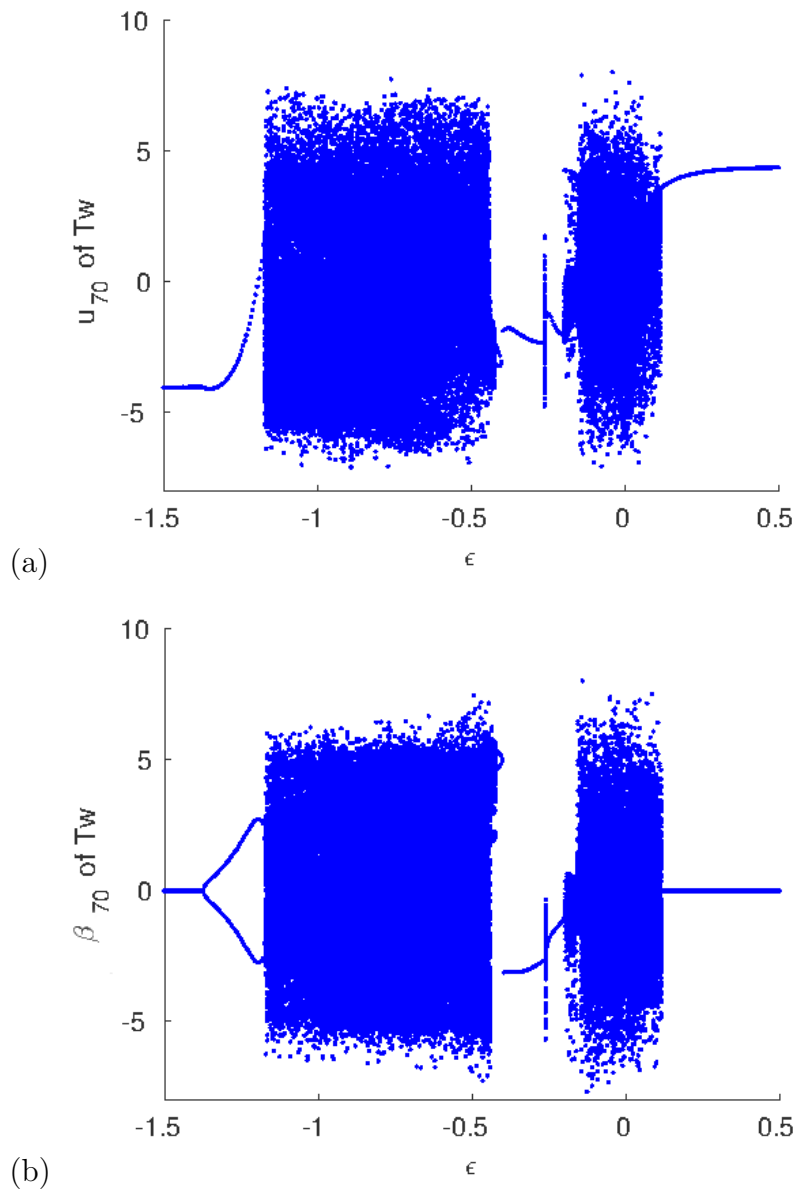
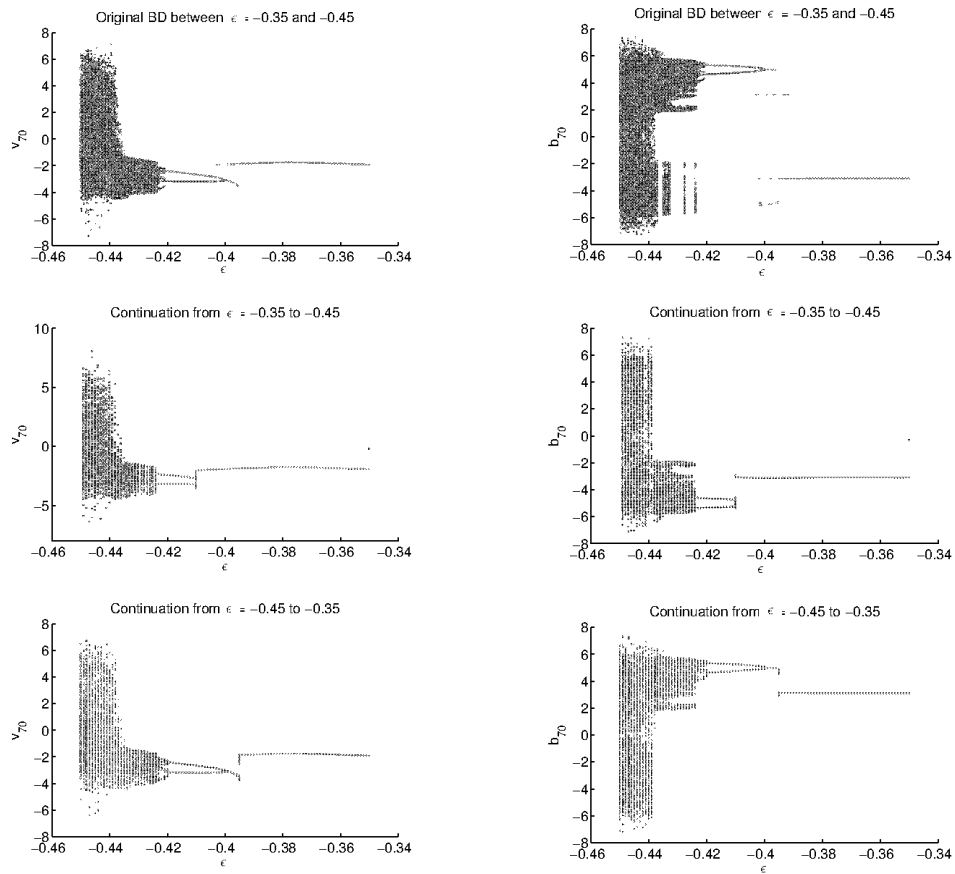


Figure 5.8: Bifurcation Diagrams of \mathcal{P} projected on shell variables (a) u_{70} ; (b) β_{70} . Last 200 of 1500 iterates are shown for each value of ϵ .

Figure 5.9 compares the earlier results (first row) with the results of continuation with decreasing (second row) and increasing (third row) parameter values. This reveals the coexistence of different attractors for the same values of ϵ , i.e., the multistability phenomenon. This is specially clear when one observes that, over the interval $\epsilon \in (-0.42, -0.40)$, different fixed-point and periodic attractors appear for the same parameter values when one performs a continuation of the solution with increasing and decreasing ϵ . The bifurcation diagram previously found by independently computing the attractor for each parameter value is composed now by these multiple attractors. This is specially interesting, as it shall lead to the coexistence of different asymptotic blowup scenarios in our shell model from the method we develop in the following chapter.



(a)

(b)

Figure 5.9: Bifurcation Diagrams of the Poincaré map \mathcal{P} projected on shell variables (a) u_{70} ; (b) β_{70} . From the top, diagram computed using parallel algorithm; diagram computed using continuation with decreasing values of ϵ ; diagram computed using continuation with increasing values of ϵ . Multistability (different coexisting attractors) appears in the small window $\epsilon \in (-0.42, 0.40)$.

Chapter 6

Asymptotic Blowup Solution of an MHD Shell Model

In Chapter 4, following [12] and [16], we constructed asymptotic solutions near blowup for the hydrodynamic shell model (4.1). These solutions were built upon the travelling wave solutions found for the renormalized model (4.2), its symmetries and its correspondence to the original model, given by the renormalization scheme (3.1) and (3.2). The aim of the present chapter is to extend these arguments and develop a method for the construction of asymptotic blowup solutions of the MHD shell model (2.2) from the attractors of its renormalized equivalent (3.3), which were extensively studied in Chapter 5.

6.1 Self-similar Blowup Solutions

We begin by extending Theorem 5 to the MHD shell model (2.2). As such, we consider a fixed-point (period-1) attractor w of the Poincaré Map

$$\mathcal{P}w = w. \tag{6.1}$$

From the definition (5.6), this translates to solutions with the property

$$u_{n+1}(\tau + 1/a) = u_n(\tau), \quad \beta_{n+1}(\tau + 1/a) = \beta_n(\tau), \tag{6.2}$$

where $1/a = \tau_1$ is the period determined by one iteration of the Poincaré map. Then, general solutions of (3.3) for large τ tend to the attractor in the

form of a travelling wave

$$u_n(\tau) = aU(n - a\tau), \quad \beta_n(\tau) = a\Psi(n - a\tau). \quad (6.3)$$

This wave solution travels towards larger n with constant positive speed a . Note that a in (6.3) is related to symmetry (S.R.1)

$$\tau \mapsto \frac{\tau}{a}, \quad u_n \mapsto au_n, \quad \beta_n \mapsto a\beta_n. \quad (6.4)$$

Thus, with no loss of generality, we can take $a = 1$ in further analysis.

Figure 5.4 depicts one such travelling wave solution. Note that the waves for both u_n and β_n travel with the same speed, as otherwise the attractor w would not be a fixed point. Under such assumptions, it is quite straightforward to extend Theorem 5. As a result, we show that both shell variables have the same scaling exponents.

Theorem 6 *Taking $a = 1$ in (6.3), let us define the scaling exponent*

$$y = \frac{1}{\log h} \int_0^1 R(\tau) d\tau \quad (6.5)$$

and the functions

$$V(t-t_c) = \exp\left(\int_0^\tau R(\tau) d\tau\right) U(-\tau), \quad B(t-t_c) = \exp\left(\int_0^\tau R(\tau) d\tau\right) \Psi(-\tau), \quad (6.6)$$

where τ is related to t by (3.1) and $R(\tau)$ is given by (3.6).

If $y > 0$, then the solution $(v_n(t), b_n(t))$ associated with (6.3) is given by

$$v_n(t) = k_n^{y-1} V(k_n^y(t - t_c)), \quad b_n(t) = k_n^{y-1} B(k_n^y(t - t_c)). \quad (6.7)$$

This solution blows up at finite time

$$t_c = \int_0^\infty \exp\left(-\int_0^{\tau'} R(\tau'') d\tau''\right) d\tau'. \quad (6.8)$$

Proof: We will follow the same steps as in the proof of Theorem 5, but with extra detail related to the presence of the magnetic field variables b_n and β_n . We begin by proving that there is in fact blowup, i.e. that integral (6.8) converges. From (6.3) and (3.3), we conclude that $R(\tau)$ must be periodic

with period $1/a = 1$. Then, from definition (6.5), a constant D can be found satisfying the inequality

$$\int_0^\tau R(\tau') d\tau' > D + \tau y \log h. \quad (6.9)$$

This inequality, applied to the definition of t_c , leads to the desired result for every positive y

$$t_c < \int_0^\infty \exp(-D - \tau y \log h) < \infty. \quad (6.10)$$

From the definitions of y in (6.5) and $k_n = h^n$, as well as the periodicity of $R(\tau)$, it is easy to verify that, for all positive τ ,

$$k_n^y = \exp\left(\int_\tau^{\tau+n} R(\tau') d\tau'\right). \quad (6.11)$$

Let us study time t' correspondent to $\tau + n$. Using definitions (3.1), (6.8) and the change of variables $\tau' = \hat{\tau} + n$,

$$\begin{aligned} t_c - t' &= \int_{\tau+n}^\infty \exp\left(-\int_0^{\tau'} R(\tau'') d\tau''\right) d\tau' = \int_\tau^\infty \exp\left(-\int_0^{\hat{\tau}+n} R(\tau'') d\tau''\right) d\hat{\tau} \\ &= \int_\tau^\infty \exp\left(-\int_0^{\hat{\tau}} R(\tau'') d\tau'' - \int_{\hat{\tau}}^{\hat{\tau}+n} R(\tau'') d\tau''\right) d\hat{\tau}. \end{aligned} \quad (6.12)$$

Comparing with (6.11), we arrive at

$$t_c - t' = k_n^{-y}(t_c - t). \quad (6.13)$$

Similarly, using (3.2), (6.11), (6.3) and definition (6.6), we have

$$\begin{aligned} v_n(t') &= k_n^{-1} \exp\left(\int_0^{\tau+n} R(\tau') d\tau'\right) u_n(\tau + n) \\ &= k_n^{y-1} \exp\left(\int_0^\tau R(\tau') d\tau'\right) U(-\tau) = k_n^{y-1} V(t - t_c) \\ b_n(t') &= k_n^{-1} \exp\left(\int_0^{\tau+n} R(\tau') d\tau'\right) \beta_n(\tau + n) \\ &= k_n^{y-1} \exp\left(\int_0^\tau R(\tau') d\tau'\right) \Psi(-\tau) = k_n^{y-1} B(t - t_c). \end{aligned} \quad (6.14)$$

Substituting (6.13) into (6.14), we obtain the identity (6.7). Expression (6.9) also implies that

$$\exp\left(\int_0^\tau R(\tau')d\tau'\right) \rightarrow \infty \quad \text{as } \tau \rightarrow \infty. \quad (6.15)$$

According to (3.2) and (6.3), this yields an unbounded norm $\|v'\|_\infty$ for $t \rightarrow t_c^-$, i.e., the solution indeed blows up at $t = t_c$, by Theorem 2. \square

Note that the functions $V(\xi)$ and $\Psi(\xi)$, as well as the scaling exponent y , do not depend directly on initial conditions. They are defined solely by the attractor of the Poincaré map developed under the used model parameters. In this sense, asymptotic solutions (6.7) are uniquely defined up to attractor symmetries if there is only one attractor. As was noted in the previous chapter, there is a multistable parameter window in the renormalized shell model (3.3). In this case, we have different coexisting asymptotic solutions, corresponding to the multiple attractors developed for such parameter values. The selection of which attractor a solution follows is then subject to the initial conditions.

Using symmetry (*S.R.1*), one can write the asymptotic formula (6.7) for any wave speed a as

$$v_n(t) = ak_n^{y-1}V(ak_n^y(t - t_c)), \quad b_n(t) = ak_n^{y-1}B(ak_n^y(t - t_c)). \quad (6.16)$$

6.2 Periodic Blowup Solutions

Let us consider a p -periodic attractor w of the Poincaré Map, with p being a positive integer,

$$\mathcal{P}^p w = w. \quad (6.17)$$

If p/a is the time period of \mathcal{P}^p , then $p/a = \tau_p$ in the definition (5.8) of the transfer operator \mathcal{T}^p takes us to a Poincaré section on which our solution follows the same profile, only shifted p shells to the right. Through this observation, we select the times τ_n which correspond to the passage between Poincaré sections satisfying the periodic condition (6.17). Explicitly, this subsequence of τ_n must satisfy the conditions,

$$\tau_n = \tau_j + Np/a, \quad n = j + pN, \quad \text{for } j = 0, \dots, p-1 \quad \text{and } j = N = 0, 1, \dots \quad (6.18)$$

Then, considering (5.8),

$$u_{n+p}(\tau + p/a) = u_n(\tau), \quad \beta_{n+p}(\tau + p/a) = \beta_n(\tau). \quad (6.19)$$

General solutions of (3.3) satisfying this condition may be written as

$$u_n(\tau) = aU_j(n - a\tau), \quad \beta_n(\tau) = a\Psi_j(n - a\tau), \quad (6.20)$$

for $j = 0, \dots, p-1$ satisfying $n = j + pN$ for some integer N . We again consider $a = 1$ without loss of generality due to symmetry (S.R.1).

An example of such a pulsating travelling wave may be found in Figure 5.5. It is interesting to note that, in general, shell variables present different periods. In the previous example, u_n is 1-periodic while β_n is 2-periodic, with the whole attractor having the common period 2.

Theorem 7 Taking $a = 1$ in (6.20), let us define the scaling exponent upon a time period of the solution as

$$y = \frac{1}{p \log h} \int_0^p R(\tau) d\tau, \quad (6.21)$$

and the functions

$$V_j(t-t_c) = \exp\left(\int_0^\tau R(\tau) d\tau\right) U_j(-\tau), \quad B_j(t-t_c) = \exp\left(\int_0^\tau R(\tau) d\tau\right) \Psi_j(-\tau) \quad (6.22)$$

for $j = 0, \dots, p-1$, where τ is related to t by (3.1) and $R(\tau)$ is given by (3.6).

If $y > 0$, then the solution $(v_n(t), b_n(t))$ associated with (6.20) is given by

$$v_n(t) = k_n^{y-1} V_j(k_n^y(t-t_c)), \quad b_n(t) = k_n^{y-1} B_j(k_n^y(t-t_c)), \quad n = j + Np. \quad (6.23)$$

This solution blows up at finite time

$$t_c = \int_0^\infty \exp\left(-\int_0^{\tau'} R(\tau'') d\tau''\right) d\tau'. \quad (6.24)$$

Proof: From (6.20) and (3.3), we conclude that $R(\tau)$ must be periodic with period $p/a = p$. Then, from definition (6.21), a constant D can be found satisfying the inequality

$$\int_0^\tau R(\tau') d\tau' > D + \tau y \log h. \quad (6.25)$$

Applying this inequality to the definition of t_c , we conclude that for every positive y ,

$$t_c < \int_0^\infty \exp(-D - \tau y \log h) < \infty. \quad (6.26)$$

From the definitions of y in (6.21) and $k_n = h^n$, as well as the periodicity of $R(\tau)$, it is easy to verify that, for all positive τ ,

$$k_{np}^y = \exp\left(\int_\tau^{\tau+np} R(\tau') d\tau'\right). \quad (6.27)$$

Let us study time t' correspondent to the passage of n renormalized time periods, $\tau + np$. Using definitions (3.1), (6.24) and the change of variables $\tau' = \hat{\tau} + np$ we derive

$$\begin{aligned} t_c - t' &= \int_{\tau+np}^\infty \exp\left(-\int_0^{\tau'} R(\tau'') d\tau''\right) d\tau' = \int_\tau^\infty \exp\left(-\int_0^{\hat{\tau}+np} R(\tau'') d\tau''\right) d\hat{\tau} \\ &= \int_\tau^\infty \exp\left(-\int_0^{\hat{\tau}} R(\tau'') d\tau'' - \int_{\hat{\tau}}^{\hat{\tau}+np} R(\tau'') d\tau''\right) d\hat{\tau}. \end{aligned} \quad (6.28)$$

Comparing this result with (6.27), we conclude that

$$t_c - t' = k_{np}^{-y}(t_c - t). \quad (6.29)$$

Similarly, using (3.2), (6.27), (6.20) and definition (6.22)

$$\begin{aligned} v_n(t') &= k_n^{-1} \exp\left(\int_0^{\tau+np} R(\tau') d\tau'\right) u_n(\tau + np) \\ &= k_n^{y-1} \exp\left(\int_0^\tau R(\tau') d\tau'\right) U_j(-\tau) = k_n^{y-1} V_j(t - t_c) \\ b_n(t') &= k_n^{-1} \exp\left(\int_0^{\tau+np} R(\tau') d\tau'\right) \beta_n(\tau + np) \\ &= k_n^{y-1} \exp\left(\int_0^\tau R(\tau') d\tau'\right) \Psi_j(-\tau) = k_n^{y-1} B_j(t - t_c), \end{aligned} \quad (6.30)$$

where the positive integer j satisfies conditions (6.18). Substituting (6.29) into (6.30), we obtain the identity (6.23). Expression (6.25) also implies that

$$\exp\left(\int_0^\tau R(\tau') d\tau'\right) \rightarrow \infty \quad \text{as } \tau \rightarrow \infty. \quad (6.31)$$

Equations (3.2) and (6.20) lead to an unbounded norm $\|v'\|_\infty$ for $t \rightarrow t_c^-$, concluding that the solution blows up at $t = t_c$, by Theorem 2. \square

Resorting to symmetry (*S.R.1*), we can write the asymptotic formula (6.23) for j satisfying (6.18) and wave speed a as

$$v_n(t) = ak_n^{y-1}V_j(ak_n^y(t - t_c)), \quad b_n(t) = ak_n^{y-1}B_j(ak_n^y(t - t_c)). \quad (6.32)$$

Figure 6.1 compared these asymptotic solutions to the direct numerical solutions of (2.2), portraying the 8th to 15th shells. The concordance between them is very satisfactory.

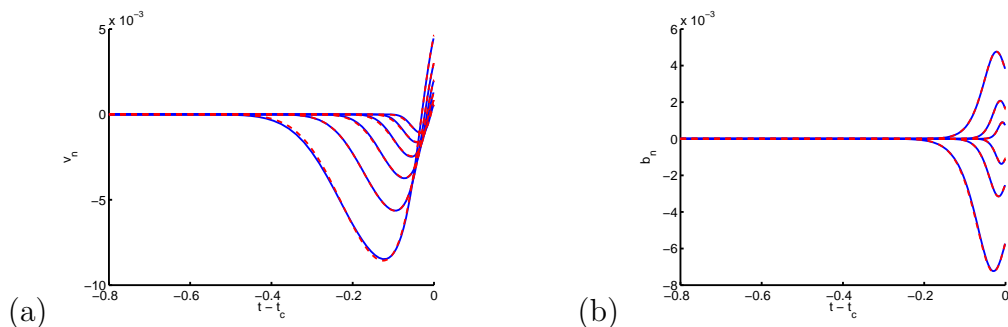


Figure 6.1: Asymptotic solutions (6.32) for $\epsilon = -1.3$ in dashed red lines; solid blue lines depict numerical solutions of (2.2).

6.3 Chaotic Blowup Solutions

In Chapter 5, we observed multiple parameter windows that develop chaotic attractors. Solutions of (3.3) which belong to these attractor do not develop a repeating wave profile, an important aspect in our construction of asymptotic solutions for self-similar and periodic solutions. It is then natural that we do not expect to develop asymptotic solutions that precisely agree to the wave profile seen in the direct numerical solutions. However, we have observed (as in Figure 5.6) that not only the solutions on the chaotic attractor are bounded, as expected from construction, but this bound is clearly defined by a wave envelop. As such, even though we might not be able to use our asymptotic solutions to a direct prediction, we may consider chaotic attractors in such a way that they will adequately describe asymptotic scaling of the blowup. These scaling properties are a central issue in other applications,

such as the study of the spectra of developed turbulence in the inertial range (see [17]), hence justifying our interest in the development of these asymptotic solutions.

It is natural, however, that we need to redefine some quantities in a statistical sense, like wave speed a and the scaling exponent y , so that they conform to the chaos of the solutions upon which they are built. We then write,

$$\frac{1}{a} = \lim_{n \rightarrow \infty} \frac{\tau_n}{n} > 0, \quad \langle A \rangle = \lim_{n \rightarrow \infty} \frac{1}{\tau_n} \int_0^{\tau_n} A(\tau) d\tau, \quad y = \frac{\langle A \rangle}{a \log h}, \quad (6.33)$$

where $1/a$ accounts for the mean time step $\langle \tau_n - \tau_{n-1} \rangle$ of the Poincaré map and $\langle A \rangle$ is the mean value of $A(\tau)$ on its attractor. We again point to the fact that, as was the case with the fixed-point and periodic attractors, the value of a may be made arbitrary due to the time-scaling symmetry. With no loss of generality we choose $a = 1$ in our analysis, and this transformation does not alter the value of y , because $A \sim a$ possesses the same scaling.

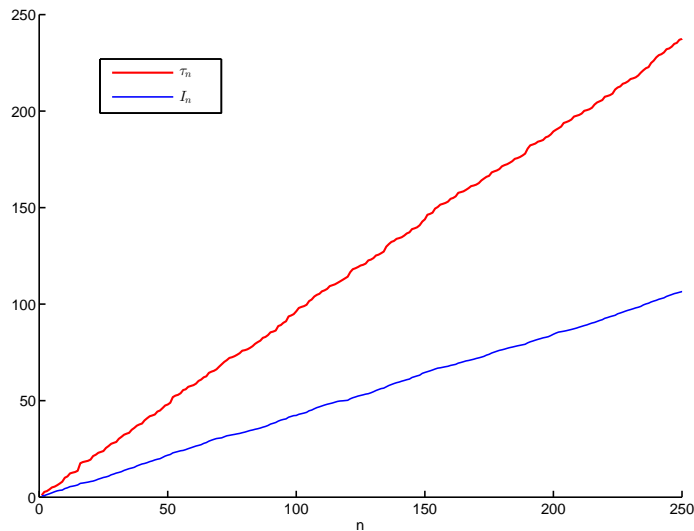


Figure 6.2: For $\epsilon = -0.8$, shown are the times τ_n and integrals $I_n = \int_0^{\tau_n} A(\tau) d\tau$ corresponding to n iterations of the Poincaré map.

Figure 6.2 shows times τ_n and integrals $\int_0^{\tau_n} A(\tau)d\tau$ corresponding to n iterations of the Poincaré map, correspondent to the chaotic attractor found for $\epsilon = -0.8$. As one may observe, these values grow linearly with n , up to small chaotic oscillations. This property is shared by our chaotic attractors in general and not only supports definitions (6.33), but also provides us with a way of computing the values of a and y . The red curve portraying τ_n has slope $1/a$, while the blue curve of I_n follows a slope of ay . As illustrated by Figure 6.2, $A(\tau) = \langle A \rangle + \delta A(\tau)$, where $\delta A(\tau)$ oscillates near a zero mean value. Then, written for $a = 1$, the inequality

$$\int_0^\tau R(\tau')d\tau' > D + \tau y \log h \quad (6.34)$$

holds and, consequently, the integral

$$t_c = \int_0^\infty \exp\left(-\int_0^{\tau'} R(\tau'')d\tau''\right) d\tau' \quad (6.35)$$

converges for $y > 0$ in a similar way as in Theorems 6 and 7, providing the value of the blowup time t_c .

Solutions of the renormalized system (3.3) may be viewed as waves travelling towards larger values of n in the logarithmic axis. The same holds for solutions associated to chaotic attractors, except that chaotically pulsating waves are developed. As an iteration of the Poincaré map corresponds to the increase of wave center position by one shell number, the mean wave speed equates to the newly defined a . From (6.33) we estimate

$$\exp\left(\int_0^{\tau_n} A(\tau)d\tau\right) = e^{\langle A \rangle \tau_n} \exp\left(\int_0^{\tau_n} \delta A(\tau)d\tau\right) \sim e^{\langle A \rangle \tau_n} \sim e^{\langle A \rangle n/a} \sim k_n^a. \quad (6.36)$$

Accordingly, we use the renormalization scheme (3.2) and (6.36) to estimate the orders of magnitude of shell solutions near blowup

$$\begin{aligned} v_n &= k_n^{-1} \exp\left(\int_0^{\tau_n} A(\tau)d\tau\right) u_n \sim k_n^{y-1}, \\ b_n &= k_n^{-1} \exp\left(\int_0^{\tau_n} A(\tau)d\tau\right) \beta_n \sim k_n^{y-1}. \end{aligned} \quad (6.37)$$

The scaling laws (6.37) are the same as the ones based on fixed-point and periodic attractors. In fact, the above arguments may be viewed as extensions of the construction of self-similar and periodic asymptotic solutions

presented earlier in this chapter. Note that this extension should also be valid for solutions belonging to quasi-periodic attractors (if such attractors are detected). Since $y > 0$, as shown in Figure 6.2, the estimates (6.37) lead to infinitely large values of $k_n v_n(t)$ as $t \rightarrow t_c^-$, confirming that solutions of (2.2) based on a chaotic attractors of the Poincaré map of (3.3) indeed blowup according to the Theorem 2.

Chapter 7

Conclusion

In this dissertation, we study a blowup phenomenon (a singularity forming in finite time) for a class of simplified turbulence models (shell models) represented by an infinite system of coupled ordinary differential equations.

Having defined suitable norms, we proved a blowup criterion for a magnetohydrodynamic shell model of turbulence, in a spirit of the Beale-Kato-Majda theorem. Then, we developed the renormalization scheme, which takes blowup time to infinity and enables the use of dynamical system methods, such as Poincaré maps, attractors and bifurcation diagrams, for identification and analysis of the blowup phenomenon. We followed with an extensive numerical study of the solutions of this renormalized system, providing self-similar, periodic and chaotically pulsating traveling waves as limiting solutions related to the fixed-point, periodic and chaotic attractors of the associated Poincaré map.

We made use of the symmetries of the shell model and its renormalized equivalent, as well as the Poincaré map attractors, to construct universal asymptotic solutions of the shell model near its blowup. We note that these asymptotic solutions describe the blowup structure, providing the scaling laws of the solutions near blowup.

From the attractors of the Poincaré maps defined for the solutions of the renormalized system, we built their bifurcation diagrams. Investigating the discontinuity of these bifurcation diagrams, we discovered a parameter interval over which multiple attractors coexist. In particular, a solution may tend to a fixed-point or a periodic attractor, depending on the initial conditions. The later leads to concurrent types of asymptotic blowup solutions. To our knowledge, this is the first observation of multistability of blowup in fluid turbulence models.

Bibliography

- [1] A.V.Babanin. *Breaking and dissipation of ocean surface waves*. Cambridge University Press, 2011.
- [2] P.Ditlevsen. *Turbulence and Shell Models*. Cambridge University Press, 2010.
- [3] L.Landau; E.Lifschitz. *Fluid Mechanics: Vol 6 (Course of Theoretical Physics)*. Butterworth-Heinemann, 1987.
- [4] D.Biskamp. *Nonlinear magnetohydrodynamics*. Cambridge Monographs on Plasma Physics. CUP, 1997.
- [5] D.Biskamp. *Magnetohydrodynamic turbulence*. Cambridge University Press, 2003.
- [6] F.Plunian; R.Stepanov; P.Frick. Shell models of magnetohydrodynamic turbulence. *Physics Reports*, 523, 2 2013.
- [7] J.Smoller. *Shock Waves and Reaction—Diffusion Equations*. Springer-Verlag, 2nd edition, 1983.
- [8] J.Gibbon; M.Bustamante; R.Kerr. The three-dimensional Euler equations: singular or non-singular? *Nonlinearity*, 21, 08 2008.
- [9] C.Gloaguen; J.Léorat; A.Pouquet; R.Grappin. A scalar model for mhd turbulence. *Physica D: Nonlinear Phenomena*, 17:154–182, 1985.
- [10] A.Obukhov. On some general characteristic of the equations of the dynamics of the atmosphere. *Fizika Atmosfery i Okeana*, 1(7):695–704, 1971.

- [11] V.Desnianskii; E.Novikov. Simulation of cascade processes in turbulent flows. *Prikladnaia Matematika i Mekhanika*, 1(38):507–513, 1974.
- [12] A.A.Mailybaev. Bifurcations of blowup in inviscid shell models of convective turbulence. *Nonlinearity*, 1(26):1105–1124, 2013.
- [13] P.Constantin; B.Levant; E.S.Titi. Regularity of inviscid shell models of turbulence. *Phys. Rev. E*, 1(75):16304, 2007.
- [14] J.T.Beale; T.Kato; A.Majda. Remarks on the breakdown of smooth solutions for the 3-d euler equations. *Communications in Mathematical Physics*, 94, 1984.
- [15] A.A.Mailybaev. Spontaneous Stochasticity of Velocity in Turbulence Models. *Multiscale Modeling & Simulation*, 14(1):96–112, 2016.
- [16] T.Dombre; J.Gilson. Intermittency, chaos and singular fluctuations in the mixed obukhov-novikov shell model of turbulence. *Physica D: Nonlinear Phenomena*, 111:265–287, 1998.
- [17] A.A.Mailybaev. Computation of anomalous scaling exponents of turbulence from self-similar instanton dynamics. *Phys. Rev. E*, 86, 8 2012.

Publications and Conference Presentations

Publication

- G.T.Goedert, V.C. Andrade, A.A. Mailybaev. Renormalization approach to blowup in inviscid MHD Shell Model. *Physicae Organum*, Universidade de Brasília, vol.I, no.I, 2015.

Conference presentations

- Ist Physics School Roberto A. Salmeron, University of Brasília, 2012.
 - Poster presentation: "Fenômenos caóticos e eventos extremos em modelos Shell de Turbulência em HD e MHD com aplicação em astrofísica".
- 29th Brazilian Colloquium in Mathematics, IMPA, Rio de Janeiro, 2012.
 - Poster presentation: "Renormalization approach to blow up in inviscid shell model of MHD Turbulence".
- Xth Scientific Initiation Congress of the Federal District, Brasília, 2013.
 - Poster presentation: "Renormalization approach to blow up in inviscid shell model of MHD Turbulence".
 - Honorary mention in the "Best exact science presentation" category.

- VIIth National Symposium in Mathematics and Scientific Initiation Journey, IMPA, 2014.
 - Short presentation: "Renormalization approach to blow up in inviscid shell model of MHD Turbulence".
 - Presentation awarded with a Silver Medal.
- IVth Workshop on Fluids and PDE's, IMPA, Rio de Janeiro, 2014.
 - Poster presentation: "Renormalization approach to blow up in inviscid shell model of MHD Turbulence".
- 8th European Postgraduate Fluid Dynamics Conference, warsaw, 2016.
 - Oral presentation: "Asymptotic blowup solutions in a MHD shell model".